www.sciencemag.org/content/346/6205/65/suppl/DC1

Supplementary Materials for

New global marine gravity model from CryoSat-2 and Jason-1 reveals buried tectonic structure

David T. Sandwell,* R. Dietmar Müller, Walter H. F. Smith, Emmanuel Garcia, Richard Francis

*Corresponding author. E-mail: dsandwell@ucsd.edu

Published 3 October 2014, *Science* **346**, 65 (2014)
DOI: 10.1126/science.1258213

This PDF file includes:

Supplementary Text

Gravity Anomaly Recovery

Gravity anomalies are small differences in the pull of gravity associated with lateral variations in mass. The best approach to measuring marine gravity is to mount a very precise accelerometer on a ship. Unfortunately this ship coverage of the oceans is very sparse *(20)*. A second, now equally precise approach is to use an orbiting radar to measure the topography of the ocean surface, which is nearly an equipotential surface. The methods for recovering maps of marine gravity anomaly from radar altimeter data are discussed in many previous publications [e.g., *(21-24)*]. Some of the key technology developments related to this new marine gravity model are provided in two recent publications *(25, 26)*. For our investigation of crustal structure we use Laplace's equation to construct the first and second vertical derivatives of the potential called gravity anomaly and vertical gravity gradient, respectively. Images of these two fields over the South Atlantic Basin are shown in Fig. 1. The full resolution maps are best viewed using a computer display program such as Google Earth. The reader can download two small KMZ files to bring these full resolution maps into their computer. In addition they can download the gridded files to construct custom maps from http://topex.ucsd.edu/WWW_html/mar_grav.html .

Improved Radar Technology

The most important contribution of the new altimeters is related to a 1.25 times improvement in range precision *(26)*. This improvement is mainly related to an increase in the pulse repetition frequency (PRF) of the newer altimeters with respect to the older altimeters. The coherent nature of the radar signal results in speckle in the echoes, which masks the echo waveform and leads to imprecision in retrieval of its parameters. This can be alleviated by averaging successive echoes, but only up to the point that they become correlated, the onset of which has been generally assumed at a PRF of somewhat above 2 kHz at the common transmitter frequency of 13.5 GHz *(27)*. The newer altimeters CryoSat-2 and Jason-1 have PRFs of 1950 Hz and 2060 Hz, respectively while the older instruments were technologically limited to lower values of 1020 Hz. Theoretically this approximate doubling of PRF should result in a $\sqrt{2} = 1.41$ improvement in range precision; the actual improvement is somewhat smaller (1.25) perhaps reflecting the onset of echo correlation at the 2 kHz PRF. Nevertheless, this improvement in range precision maps directly into an improvement in gravity field accuracy.

CryoSat-2 was also operated in a new Synthetic Aperture Radar (SAR) mode over very limited areas of the oceans. This mode has a much higher PRF of 18.2 kHz and the highly correlated echoes are summed coherently in bursts of 64 pulses to form a long synthetic aperture. This enhances along-track resolution in the form of a set of narrow beams distributed in the along-track direction *(27–30)*. Unlike the conventional pulse-width limited geometry, the resulting echo waveforms have useful information in both the leading and trailing edges. This, together with an increase in the effective number of independent samples resulting from the SAR technique, reduces the height noise by a factor of ~1.4 compared to conventional LRM *(31)*. Comparison of height noise performance *(26)* indeed shows this expected improvement for CryoSat-2's SAR but similar gains for pulse-width limited echoes are obtained by a two-pass processing

scheme in which the slowly varying ocean wave-height is first estimated and smoothed and then excluded from the estimation process in the second pass. These results show that CryoSat-2's LRM performs slightly better than Jason-1 (which is already excellent), despite its reduced PRF. Much of the design of the two radars is common but it is likely that the improvements introduced for CryoSat-2's mission, particularly the higher transmitter power needed for operation over sloping ice surfaces and the extreme phase stability required for SAR interferometry, are contributing to this performance.

Coherence-Enhancing Filter

Despite the advances in satellite gravity anomaly image quality described in this paper, some high-frequency noise remains. In order to further improve the interpretation of linear tectonic features seen in the new vertical gravity gradient images, we have applied a filtering technique called coherence-enhancing diffusion to a selected region in the South Atlantic (Fig. 3) *(32)*. This filter combines anisotropic diffusion (a low-pass filter) with texture analysis, such that a diffusion tensor is computed from the local image structure so that the diffusion is parallel to linear features in the data. This type of filter has been successfully applied for enhancing noisy seismic reflection images to facilitate improved tracking of seismic horizons *(33)*, and is applied to vertical gravity gradient data here for the first time. While high-frequency noise has been suppressed, linear, coherent seafloor structures have been enhanced. In particular the internal en-echelon structure of the extinct mid-ocean ridge on the African Plate has been enhanced, while the juxtaposed differences in seafloor structure west and east of the conjugate pseudofault have been enhanced as well. Deeply buried linear structures of the Santos Basin and Sao Paulo Plateau offshore Brazil have been equally enhanced (Fig. 3), illustrating that improved satellite data combined with well-targeted filtering have a great potential to reveal previously hidden structures on abyssal plains and along passive margins.

Gravity Anomaly Uncertainty

We estimated the uncertainty in the gravity by calculating the rms difference in slope between individual altimeter profiles and the mean north and east slopes used to compute gravity (Fig S1.) The uncertainties were calibrated by comparisons with shipboard data from two completely different proprietary sources. First we computed the rms difference between the altimeter-derived gravity and more accurate shipboard gravity in a small region in the Gulf of Mexico. The ship data, provided by EDCON Inc., were collected on a very fine grid and have an rms crossover error of 0.5 mGal *(25)*. For this first comparison we found an rms difference of 1.60 mGal. In the second case, the altimeter-derived gravity data were compared with 30 million of the best shipboard data by the National Geospatial Intelligence Agency (NGA personal communication) resulting in an rms difference of 2.6 mGal. The rms difference is somewhat higher (3.6 mGal) in shallow areas (< 1 km) and somewhat lower (2.3 mGal) in deeper areas (3 - 6 km). On average, the NGA ship data have an rms error of 1 - 2 mGal. Assuming the mean rms error is 1.6 mGal then the mean rms error in the altimeter-derived gravity is ~2 mGal in agreement with the calibration derived from the Gulf of Mexico comparison. As shown in our previous study *(25)* most of the error reduction between this new gravity model and the older models occur in the 12 to 40 km wavelength band.

The noise reduction over the short wavelength band provides a dramatic improvement in the clarity of the vertical VGG signals. We used the Gulf of Mexico region to illustrate this noise reduction (Fig. S2). The upper plot shows the VGG derived from only Geosat and ERS-1 altimetry data *(24)* while the middle plot shows also includes the new measurements from CryoSat-2 and Jason-1. The reduction in noise between the old and new models reveals the extinct spreading ridges and transforms as well as the continent ocean boundary. One can also see some of these features in the old model but they are largely obscured by noise. The difference between the new and old model (Fig. S2 c) reveals the noise in the old model. The rms difference between the two models is 6.9 eotvos units and in terms of gravity anomaly (not shown) the rms difference is 2.2 mGal. The rms differences are zero over land, where the VGG and gravity anomaly are set by the EGM08 model *(9)*. Differences are greatest near the shorelines where the raw altimeter waveforms are sometimes contaminated by stray echoes off the land. To understand the contribution of each of the satellite data sets to the accuracy of the gravity grid, we have constructed a suite of gravity models after removing one of the non-repeat data sets. We find that because the four non-repeat altimeter data sets have differing orbital inclinations and noise levels they are all important for achieving the best overall accuracy.

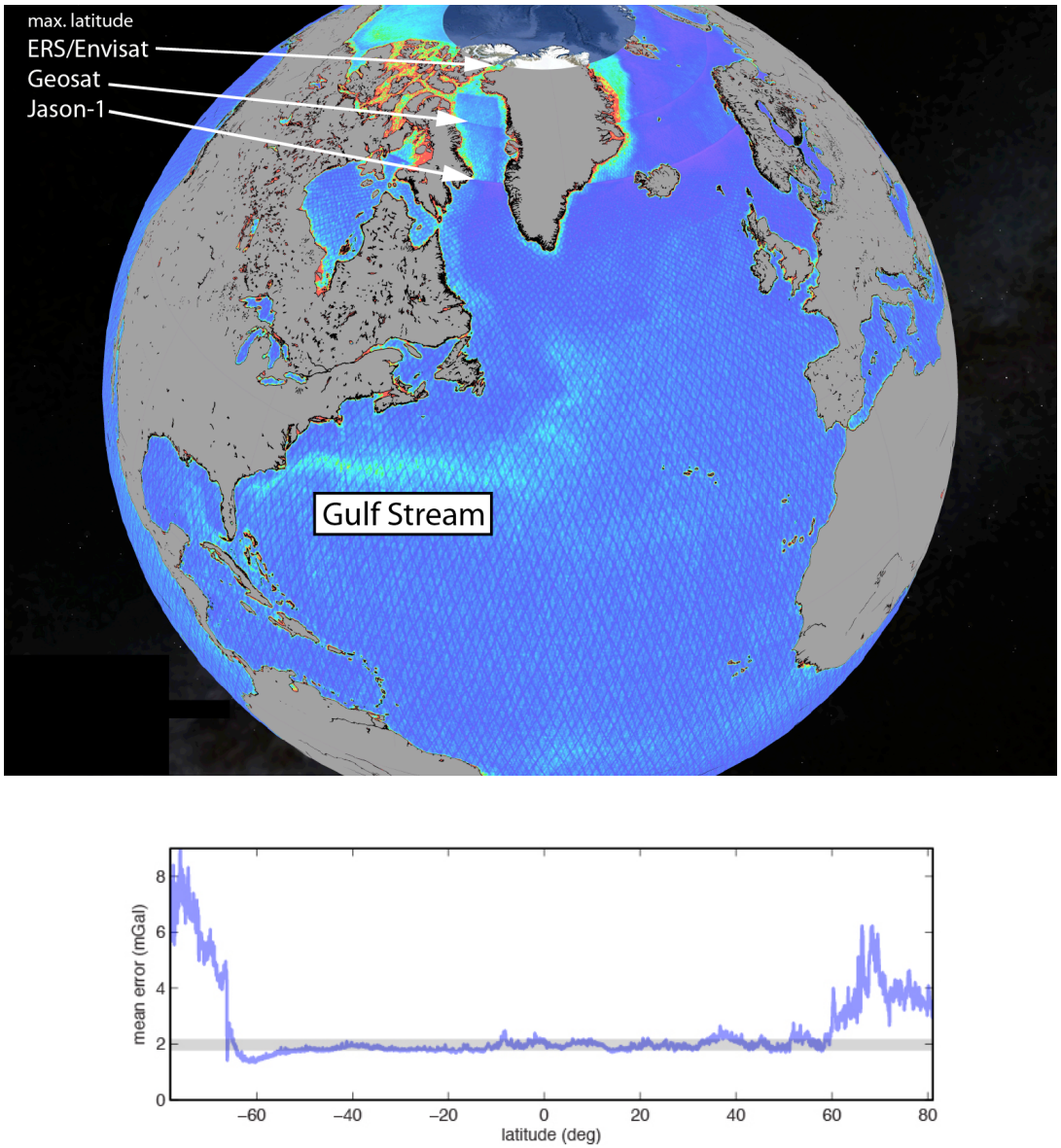

Fig. S1. Gravity error. (a) Estimated error in marine gravity anomaly to 81 degrees latitude. Color scale ranges from 0-10 mGal. Relatively larger noise occurs in areas of high mesoscale variability such as the Gulf Stream. Sharp changes in gravity noise occur at the maximum inclination of Jason-1, Geosat, ERS/Envisat ground tracks. (b) Longitude-averaged gravity error versus latitude. Noise is higher in polar regions due to lower track density and altimeter noise caused by sea ice. (Note CryoSat-2 collects data to 88 degrees latitude but this plot only extends to 81.)

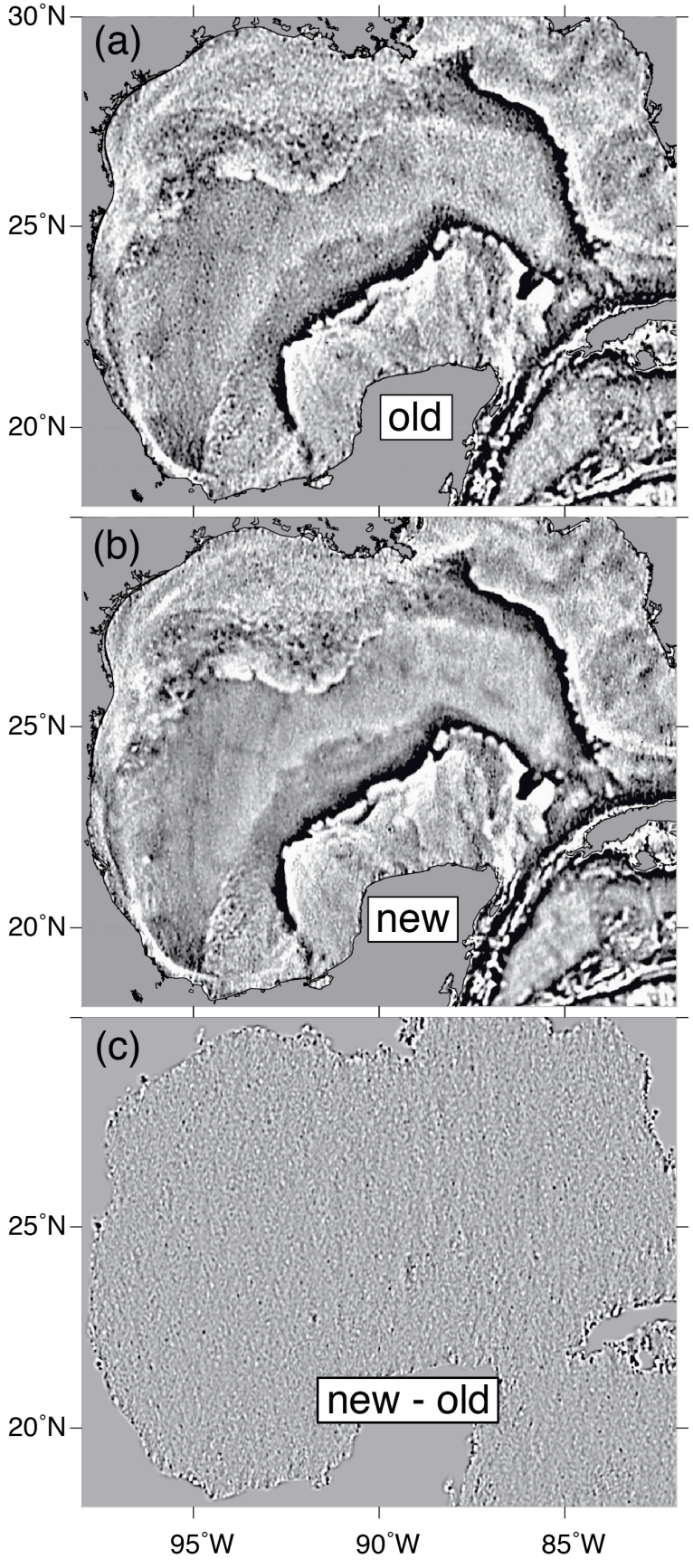

Fig. S2. Gulf of Mexico VGG. (a) Old VGG model based on Geosat and ERS-1. (b) New VGG model also includes data from CryoSat-2 and Jason-1. (c) Difference between the two models plotted using the same greyscale shows noise in the old VGG model. Mercator projection, grey scale saturates at +/- 20 eotvos units.

References and Notes

1. J. T. Wilson, A new class of faults and their bearing on continental drift. *Nature* **207**, 343–347 (1965). doi:10.1038/207343a0

2. S. Cande, J. LaBrecque, W. Haxby, Plate kinematics of the South Atlantic: Chron C34 to present. *J. Geophys. Res. Solid Earth* **93**, 13479–13492 (1988). doi:10.1029/JB093iB11p13479

3. C. Heine, J. Zoethout, R. D. Müller, Kinematics of the South Atlantic rift. *Solid Earth* **4**, 215–253 (2013). doi:10.5194/se-4-215-2013

4. L. A. Lawver, L. M. Gahagan, I. W. Dalziel, A tight fit—Early Mesozoic Gondwana, a plate reconstruction perspective. *Mem. Natl. Inst. Polar Res.* **53**, 214–229 (1998).

5. M. S. Steckler, A. B. Watts, Subsidence of the Atlantic-type continental margin off New York. *Earth Planet. Sci. Lett.* **41**, 1–13 (1978). doi:10.1016/0012-821X(78)90036-5

6. C. S. Liu, D. T. Sandwell, J. R. Curray, The negative gravity field over the 85°E Ridge. *J. Geophys. Res.* **87**, 7673–7686 (1982). doi:10.1029/JB087iB09p07673

7. K. Matthews, R. D. Müller, P. Wessel, J. M. Whittaker, The tectonic fabric of the ocean basins. *J. Geophys. Res. Solid Earth* **116**, 1–28 (2011). doi:10.1029/2011JB008413

8. Materials and methods are available as supplementary materials on *Science* Online.

9. J. Pindell, L. Kennen, in *The Geology and Evolution of the Region Between North and South America*, K. James, M. A. Lorente, J. Pindell, Eds. (Special Publication, Geological Society of London, London, 2009), vol. 328, pp. 1–55.

10. C. O'Neill, R. D. Müller, B. Steinberger, On the uncertainties in hot spot reconstructions and the significance of moving hot spot reference frames. *Geochem. Geophys. Geosyst.* **6**, Q04003 (2005). doi:10.1029/2004GC000784

11. R. D. Müller, W. R. Roest, J. Y. Royer, Asymmetric sea-floor spreading caused by ridge-plume interactions. *Nature* **396**, 455–459 (1998). doi:10.1038/24850

12. R. Granot, J. Dyment, Y. Gallet, Geomagnetic field variability during the Cretaceous Normal Superchron. *Nat. Geosci.* **5**, 220–223 (2012). doi:10.1038/ngeo1404

13. W. H. F. Smith, D. T. Sandwell, Global seafloor topography from satellite altimetry and ship depth soundings. *Science* **277**, 1956–1962 (1997). doi:10.1126/science.277.5334.1956

14. J. A. Goff, W. H. F. Smith, K. A. Marks, The contributions of abyssal hill morphology and noise to altimetric gravity fabric. *Oceanography* **17**, 24–37 (2004). doi:10.5670/oceanog.2004.64

15. N. K. Pavlis, S. A. Holmes, S. C. Kenyon, J. K. Factor, The development and evaluation of the Earth Gravitational Model 2008 (EGM2008). *J. Geophys. Res.* **117**, B04406 (2012). 10.1029/2011JB008916 doi:10.1029/2011JB008916

16. M. Seton, R. D. Müller, S. Zahirovic, C. Gaina, T. Torsvik, G. Shephard, A. Talsma, M. Gurnis, M. Turner, S. Maus, M. Chandler, Global continental and ocean basin reconstructions since 200 Ma. *Earth Sci. Rev.* **113**, 212–270 (2012). doi:10.1016/j.earscirev.2012.03.002

17. W. Mohriak, M. Nóbrega, M. Odegard, B. Gomes, W. Dickson, Geological and geophysical interpretation of the Rio Grande Rise, south-eastern Brazilian margin: Extensional tectonics and rifting of continental and oceanic crusts. *Petrol. Geosci.* **16**, 231–245 (2010). doi:10.1144/1354-079309-910

18. I. Scotchman, G. Gilchrist, N. Kusznir, A. Roberts, R. Fletcher, in *The Breakup of the South Atlantic Ocean: Formation of Failed Spreading Axes and Blocks of Thinned Continental Crust in the Santos Basin, Brazil and Its Consequences For Petroleum System Development* (Petroleum Geology Conference Series, Geological Society of London, London, 2010), pp. 855–866.

19. W. U. Mohriak, P. Szatmari, S. Anjos, Salt: Geology and tectonics of selected Brazilian basins in their global context. *Geol. Soc. London Spec. Publ.* **363**, 131–158 (2012). doi:10.1144/SP363.7

20. M. T. Chandler, P. Wessel, Improving the quality of marine geophysical track line data: Along-track analysis. *J. Geophys. Res. Solid Earth* **113**, B02102 (2008). doi:10.1029/2007JB005051

21. O. B. Andersen, P. Knudsen, Global marine gravity field from the ERS-1 and Geosat geodetic mission altimetry. *J. Geophys. Res. Oceans* **103**, 8129–8137 (1998). doi:10.1029/97JC02198

22. W. Haxby, G. Karner, J. LaBrecque, J. Weissel, Digital images of combined oceanic and continental data sets and their use in tectonic studies. *EOS* **64**, 995–1004 (1983). doi:10.1029/EO064i052p00995

23. C. Hwang, B. Parsons, An optimal procedure for deriving marine gravity from multi-satellite altimetry. *Geophys. J. Int.* **125**, 705–718 (1996). doi:10.1111/j.1365-246X.1996.tb06018.x

24. D. T. Sandwell, W. H. F. Smith, Global marine gravity from retracked Geosat and ERS-1 altimetry: Ridge segmentation versus spreading rate. *J. Geophys. Res. Solid Earth* **114**, B01411 (2009). doi:10.1029/2008JB006008

25. D. Sandwell, E. Garcia, K. Soofi, P. Wessel, M. Chandler, W. H. F. Smith, Toward 1-mGal accuracy in global marine gravity from CryoSat-2, Envisat, and Jason-1. *Leading Edge* **32**, 892–899 (2013). doi:10.1190/tle32080892.1

26. E. S. Garcia, D. T. Sandwell, W. H. F. Smith, Retracking CryoSat-2, Envisat and Jason-1 radar altimetry waveforms for improved gravity field recovery. *Geophys. J. Int*. **196**, 1402–1422 (2014).

27. D. J. Wingham, C. R. Francis, S. Baker, C. Bouzinac, D. Brockley, R. Cullen, P. de Chateau-Thierry, S. W. Laxon, U. Mallow, C. Mavrocordatos, L. Phalippou, G. Ratier, L. Rey, F. Rostan, P. Viau, D. W. Wallis, CryoSat: A mission to determine the fluctuations in Earth's land and marine ice fields. *Adv. Space Res.* **37**, 841–871 (2006). doi:10.1016/j.asr.2005.07.027

28. H. D. Griffiths, Synthetic aperture processing for full-deramp radar altimeters. *Electron. Lett.* **24**, 371–373 (1988). doi:10.1049/el:19880251

29. W. T. K. Johnson, Magellan imaging radar mission to Venus. *Proc. IEEE* **79**, 777–790 (1991). doi:10.1109/5.90157

30. R. K. Raney, The delay Doppler radar altimeter. *IEEE Trans. Geosci. Rem. Sens.* **36**, 1578–1588 (1998). doi:10.1109/36.718861

31. L. Phalippou, V. Enjolras, Re-tracking of SAR altimeter ocean power waveforms and related accuracies of sea surface height, significant wave height, and wind speed. *Proc. IEEE IGARSS'07*, 3533–3536 (2007).

32. J. Weickert, Coherence-enhancing diffusion of colour images. *Image Vis. Comput.* **17**, 201–212 (1999). doi:10.1016/S0262-8856(98)00102-4

33. G. C. Fehmers, C. F. Höcker, Fast structural interpretation with structure-oriented filtering. *Geophysics* **68**, 1286–1293 (2003). doi:10.1190/1.1598121